Biochimica et Biophysica Acta, 512 (1978) 270—283

BBA 78132

SHAPE AND STABILITY CHANGES IN HUMAN ERYTHROCYTE MEMBRANES INDUCED BY METAL CATIONS

GREGORY S.B. LIN and ROBERT I. MACEY

Group in Biophysics and Medical Physics, and Department of Physiology-Anatomy, University of California, Berkeley, Calif. 94720 (U.S.A.)

(Received January 31st, 1978)

Summary

Asymmetric human erythrocyte ghost membranes behave as bilayer couples and exhibit a radius of curvature preference depending on the state of expansion or contraction of each side of the bilayer. The inside-out preference in the absence of added metal cations is gradually reduced as the K^+ concentration is raised to 200 mM until a slight right-side-out preference may be exhibited. Divalent cations (denoted M^{2+}; Ca^{2+}, Mg^{2+} and Mn^{2+}) induce inside-out curvature at very low concentrations, right-side-out curvature at intermediate concentrations, and inside-out curvature again at high ones. This "triphasic" response is attributed to changes in the packing of acidic phospholipid (PL^-) pairs in the A-face as a function of M^{2+} : PL^- binding stoichiometry: 0 : 1 (PL^- electrostatic repulsion and A-face expansion), 1 : 2 (PL_2M crossbridging and contraction), and 1 : 1 (PLM^+ repulsion and expansion).

Generally increasing parent vesicle size is associated with higher cation concentrations. This is distinguished from the internal and external membrane blebbing preferred at different concentrations in accord with sidedness preference. Parent vesicle size was interpreted to be most closely associated with cation stabilisation (resistance to fragmentation) of the membrane, while sidedness and size (radius of curvature) of blebs were most closely correlated with packing of lipid molecules in the bilayer.

Introduction

It is well known that biological membranes can undergo a variety of local and overall changes in shape, involving changes in bilayer curvature. For example, secretory processes may take place by fusion between intracellular vesicles and the cell membrane without disrupting the basic continuity of the lipid bilayer [1—3]. The reverse process underlies phagocytosis and pinocytosis

as seen in macrophages [4]. Cells undergo shape changes at different stages in the cell cycle, or in the process of cell maturation and differentiation.

Shape changes may be induced by external agents, most notably amphipathic anaesthetics [5,6] and divalent cations [7,8]. In particular, divalent cations, such as calcium, appear to be required in intermediate concentrations for most forms of biological membrane fusion. Calcium in the concentration range 0.1—10 mM stimulates phagocytosis by cells [9] and fusion of lipid membranes [10]. Theoretical calculations [11] suggest that the close apposition of membranes required for fusion can be achieved only by microvilli with small radii of curvature, as are observed in the calcium-induced echinocyte transformation of erythrocytes [7].

That an asymmetry of biological membranes plays a role in cation-induced shape changes has been suggested by a specific dependence on intracellular calcium levels. The divalent cation ionophore A23187 has been shown to further promote membrane fusion in the presence of at least 1 mM external calcium in hen erythrocytes [12], human erythrocyte ghosts [13], and rat mast cells [14,15]. The requirement for a divalent cation, such as calcium, in the fusion of phosphatidylserine-rich liposomes [16] also suggests that the cation interaction with negative phospholipids localised on the inner face of erythrocyte membranes [17—19] is of particular importance. The nature of this binding is non-specific as indicated by the observation that metal cations of the same valence bind competitively to acidic phospholipids in erythrocyte membranes [20].

In this investigation, the effect of inorganic cations on the radius of curvature of human erythrocyte ghost membranes is examined. The relative fractions of membrane material which is right-side-out and inside-out are estimated by assaying for markers which are specifically located on one side of the membrane or the other. We make use of sialic acids on the extracellular surface (denoted as the B-face) and NADH-cytochrome *c* oxidoreductase on the cytoplasmic surface (A-face) [21]. We propose a molecular model of cation-mediated phospholipid packing as a sufficient, though not necessarily exclusive, determinant of bilayer curvature.

Human erythrocytes are neither noted for endocytotic and secretory activity, nor for morphological changes during the cell cycle since they do not divide. However, because their membranes have been by far the best characterised among biological membranes, they serve as good model systems for this study.

Materials and Methods

Preparation of membrane vesicles. White ghosts relatively free of peripheral proteins were prepared from fresh whole blood of 20—35-year-old males based on the procedure of Dodge et al. [22]. To prevent clotting, the blood was taken in either acid/citrate/dextrose or in some cases sodium heparin (to a final concentration of 4 I.U./ml). The blood was cooled to 4—7°C and EDTA added to 10 mM. The cells were centrifuged at 1200 × *g*, and the supernatant and most of the buffy coat removed. The cells were washed twice more in isotonic saline buffered in 5 mM sodium phosphate in the range pH 7.4—7.8. Hypotonic lysis was accomplished in 5 mM sodium phosphate buffer at the same tempera-

ture and pH. The suspensions were centrifuged at 23 500 × *g* for 10 min and the deep red supernatant and dark residual pellet (under the lighter ghost pellet) were vacuum aspirated. Hypotonic wash was repeated until the ghosts were essentially free of visible pink coloration. In some procedures, EDTA was added to 1 mM to reduce divalent cation crosslinking of peripheral proteins and optimise removal of both. In some other procedures, the final hypotonic wash was done in doubly distilled water to remove phosphate that would otherwise precipitate divalent cations (especially Mn^{2+}) to be added later.

Each purified erythrocyte ghost pellet was suspended for at least 1 h in 15—30 volumes of the respective experimental ionic solution buffered with either 0.5 mM sodium phosphate or tris(hydroxymethyl)aminomethane to pH 7.4—7.7. The latter was especially preferred together with Ca^{2+} or Mn^{2+} because it avoids precipitation. Moderate vesiculation was accomplished by expelling each suspension through a 27 gauge needle at least three times at 4—7°C using a 2 ml glass syringe under continuous manual pressure. Severe vesiculation which reduces all membranes to vesicular diameters on the order of 0.1 μm was accomplished by an ultrasonication probe.

Phase contrast microscopy. Pre-vesiculation and final vesicle suspensions were observed and counted according to size, shape, and density (presence of blebs or internal vesicles) without fixation or staining under a phase contrast microscope.

Freeze-fracture and freeze-etch electron microscopy. Final vesicle suspensions were centrifuged at 33 000 × *g* for 20 min at 4°C. The supernatants were vacuum aspirated, leaving dense viscous vesicle suspensions suitable for freezing without fixation on cardboard discs in liquid Freon 22 ($CHCl_2F$). The discs were stored in liquid nitrogen until ready for fracturing in a Balzers BA360M freeze-etch unit. Immediately following cutting, some specimens were etched for approx. 2 min and platinum-carbon shadow replicas made. The replicas were cleaned of tissue and mounted on grids coated with carbon-stabilised formvar films. Observations were made in a Zeiss EM-9S2 electron microscope.

Sialic acid determination. Sialic acids were cleaved from the extracellular surface of the membrane by the addition of 2 I.U. of neuraminidase (from *Vibrio cholerae*) to 0.3 ml of each final vesicle suspension. The mixture was incubated at 37°C for at least 1 h. Enzyme activity was stopped by adding 3.0 ml of cold buffer solution. The suspensions were then spun down at 23 500 × *g* for 10 min at 4°C. From each supernatant 0.3-ml aliquots were taken and sialic acid content determined according to the method of Warren [23]. To each sample was added 0.1 ml of sodium metaperiodate solution (0.2 M $NaIO_4$ in 9.0 M H_3PO_4). After allowing them to react at room temperature for at least 20 min, 1.0 ml of sodium arsenite solution (0.77 M $NaAsO_2$/0.25 M Na_2SO_4/0.05 M H_2SO_4) was added and the tubes shaken until the brown colour disappears. Then 3.0 ml of freshly prepared thiobarbituric acid solution (0.6% 2-thiobarbituric acid in 0.25 M Na_2SO_4) was added. The samples were heated in a vigorously boiling water bath for 15 min, then cooled in a cold water bath. They were vigorously vortexed with 3.0 ml of cyclohexanone and centrifuged at 2000 × *g* for 3 min. The absorbance of the upper cyclohexanone phase was read at 549 nm on either a Beckman DU or Bausch and Lomb Spectronic 700 spectrophotometer.

Assay for NADH-cytochrome c oxidoreductase accessibility. NADH-cyto-

chrome *c* oxidoreductase accessibility was determined based on the method of Steck and Kant [21,24]. However, when vesicle suspensions contain divalent cations in concentrations above 1 mM some inhibition of oxidoreductase activity was observed, consistent with previous work [25]. Therefore, samples with high levels of divalent cations were washed in buffer solution and $CaCl_2$ added back to a final concentration of 0.1 mM to avoid differential inhibition. (Such changes in divalent cation concentration were shown to induce less than 10% vesicle sidedness inversion within short durations as determined by the sialic acid method.) The 0.8-ml suspensions were brought to room temperature, and 0.2 ml of buffered 1.0 mM β-NADH solution and 0.2 ml of buffered 2.5 mg/ml oxidised cytochrome *c* (from horse heart) solution, both freshly prepared, were added. The rate of increase of absorbance was measured at 550 nm by plotting over time using a Beckman DU spectrophotometer with a chart recorder attached.

Protein determination. Vesicle suspensions were precipitated in 5% (w/w) trichloroacetic acid, cooled to 7°C, centrifuged at 3000 × *g* for 5 min, and the clear supernatant aspirated off without disturbing the pellet. The pellets were dissolved in 1.0 M NaOH at room temperature. In those experiments involving Mn^{2+} which precipitates as a hydroxide, the trichloroacetic acid/NaOH solubilisation procedure was not employed and the vesicle suspensions were used as is. Light scattering did not appear to adversely affect relative absorbance measurements. Protein content was determined according to the method of Warburg and Christian [26] by measuring absorbance (primarily of tyrosine and tryptophan) at 280 nm.

Protein content was alternatively determined by the method of Lowry et al. [27] which proved to have less temporal stability, though possibly greater potential accuracy and sensitivity.

Interpretation of vesicle sidedness. The relative accessibility of sialic acid (or of the B-face), R_{sa}, and the relative accessibility of oxidoreductase (or of the A-face), R_{cy}, can be expressed as ratios of absorbancies:

$$R_{sa} = A(\text{sialic acid})/A(\text{protein}) \quad (1)$$

$$R_{cy} = \Delta A(\text{reduced cytochrome } c)/A(\text{protein}) \quad (2)$$

The actual fraction of sialic acid accessible, F_{sa}, can then be obtained by normalising the R_{sa} values on the assumption that unvesiculated ghosts which remain whole and do not demonstrate spontaneous vesiculation are essentially all right-side-out (i.e. $F_{sa} = 1.0$). Similarly, populations of largely inside-out and unsealed vesicles have been used, though with less reliability, to provide estimates for normalising R_{cy} values to F_{cy} values, the actual fraction of oxidoreductase accessible.

For the purpose of experimentally determining the fractions of vesicles with right-side-out or inside-out sidedness orientations, four vesicle configurations need to be distinguished: (1) sealed right-side-out, (2) unsealed right-side-out, (3) unsealed inside-out, and (4) sealed inside-out. The assay for sialic acid, as a measure of the accessibility of the B-face to neuraminidase, yields the fraction F_{sa} of membrane material in configurations 1, 2 and 3. Similarly, the assay for oxidoreductase activity, representing the accessibility of the A-face to dissolved

cytochrome *c*, yields the fraction F_{cy} of membrane material in configurations 2, 3 and 4. The fraction F_{sRO} of sealed right-side-out vesicles and the fraction F_{sIO} of sealed inside-out vesicles can thereby be distinguished. However, because the assays cannot distinguish between unsealed right-side-out and unsealed inside-out vesicles, these fractions may be collectively denoted $F_{unsealed}$, where

$$F_{unsealed} = F_{sa} + F_{cy} - 1 \tag{3}$$

$$F_{sRO} = F_{sa} - F_{unsealed} = 1 - F_{cy} \tag{4}$$

$$F_{sIO} = F_{cy} - F_{unsealed} = 1 - F_{sa} \tag{5}$$

In the right-side-out sidedness plots (Fig.s 1 and 2) the principal or upper curve is F_{sa} and where given the lower curve is F_{sRO}. The actual fraction of membrane material in the right-side-out configurations (sealed and unsealed) must lie somewhere in between, or slightly below the F_{sa} curve.

Determination of median vesicle size. Vesicle suspensions in which a significant fraction of vesicles were at least 2 μm in diameter (as seen by phase contrast microscopy) were counted in two size ranges in a Particle Data Electrozone/Celloscope Model 112CLTS/ADC. This instrument, by employing an electric field across an orifice through which particles in saline solution are drawn, detects resistance pulses proportional to particle volume. Using a 48 μm orifice, vesicles of 2.1 μm diameter or greater were easily counted. By equalising the readings on a 2-channel digital counter, median vesicle volumes were obtained (taking into consideration coincidence counts). The conductivity of low ionic strength suspension media was raised to the required level by addition of up to 10 mM NaCl without causing any visible vesicle shrinkage.

Results

Effect of monovalent cations

From sialic acid assays, F_{sa} values were recorded as a function of the concentration of K^+ (KCl buffered in Na_2HPO_4) in the range 0—200 mM (Fig. 1). Potassium clearly produces a curve showing accessibility of the B-face (indicative of right-side-out sidedness) rising continuously from low to high [K^+], but rising most rapidly in the range 1—10 mM. The slight dip at 200 mM may be due to a slight decrease in right-side-out sidedness, but may also be attributable to a slight reduction in $F_{unsealed}$.

These results were correlated with observations of vesicle morphology and estimates of size distributions as seen through phase contrast microscopy and according to analysis by cell counter (Table I). The observation that the mean vesicle diameter also steadily increases with [K^+] may indicate either or both of two things: (1) K^+ increases membrane stability, i.e. resistance to fragmentation during mechanical vesiculation. (2) K^+ increases the preferred radius of curvature of the bilayer.

Effect of divalent cations on vesicle sidedness

The effects of Ca^{2+} and Mg^{2+} (buffered in Tris or phosphate) and Mn^{2+} (buffered in Tris) on vesicle sidedness and morphology were similarly observed

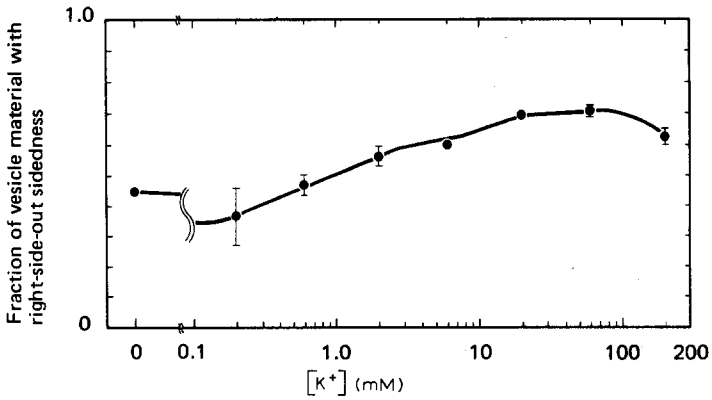

Fig. 1. Experimental fraction of vesicles which are right-side-out or unsealed as a function of bulk K^+ concentration $[K^+]$ used in the vesiculation procedure. (The values listed on the abscissa represent the initial $[K^+]$. These may differ from the equilibrium values because of ion adsorption to the membrane.) Data represent the fraction of vesicles in which the external surface (associated with the membrane B-face) is accessible to neuraminidase activity. Vertical bars represent standard errors.

in the concentration range 0—100 mM (Figs. 2 and 3). Assays were done for accessibility of both sialic acid and cytochrome *c* oxidoreductase. Both assays yield triphasic sidedness curves with the fraction of right-side-out vesicles being maximal at intermediate concentrations. The locations of the right-side-out peaks for Ca^{2+} and Mg^{2+} were nearly the same at about 3.3 and 2.8 mM, respectively, and somewhat lower for Mn^{2+} at roughly 1.2 mM. This indicates that the binding affinity of Mn^{2+} for those sites which affect membrane sidedness is somewhat greater than those of Ca^{2+} and Mg^{2+}.

Vesiculation pathway and daughter vesicle formation

Observed changes in vesicle shape suggest that the vesiculation process may actually begin before application of shear stress and that it proceeds in two phases: (1) spontaneous vesiculation and blebbing, and (2) shearing off of the blebs and further disruption during mechanical vesiculation. Under conditions

TABLE I

VESICLE SIZE DISTRIBUTION AFTER SYRINGE VESICULATION IN THE PRESENCE OF VARIOUS CONCENTRATIONS OF K^+

Vesicle diameter d is in μm; numbers following ± are standard errors.

$[K^+]$ (mM)	Percent of vesicles in size range		Median size in the range $d \geq 2.1$
	$0.1 < d < 2$	$2 \leq d \leq 7$	
0	100 ± 0	0	—
0.2	99 ± 0.2	1 ± 0.2	—
0.6	99 ± 0.5	1 ± 0.5	—
2.0	98 ± 0.5	2 ± 0.5	—
6.0	97 ± 0	3 ± 0	—
20	90 ± 0.9	10 ± 0.9	2.50
60	85 ± 5.0	15 ± 5.0	2.55
200	80 ± 2.6	20 ± 2.6	2.52

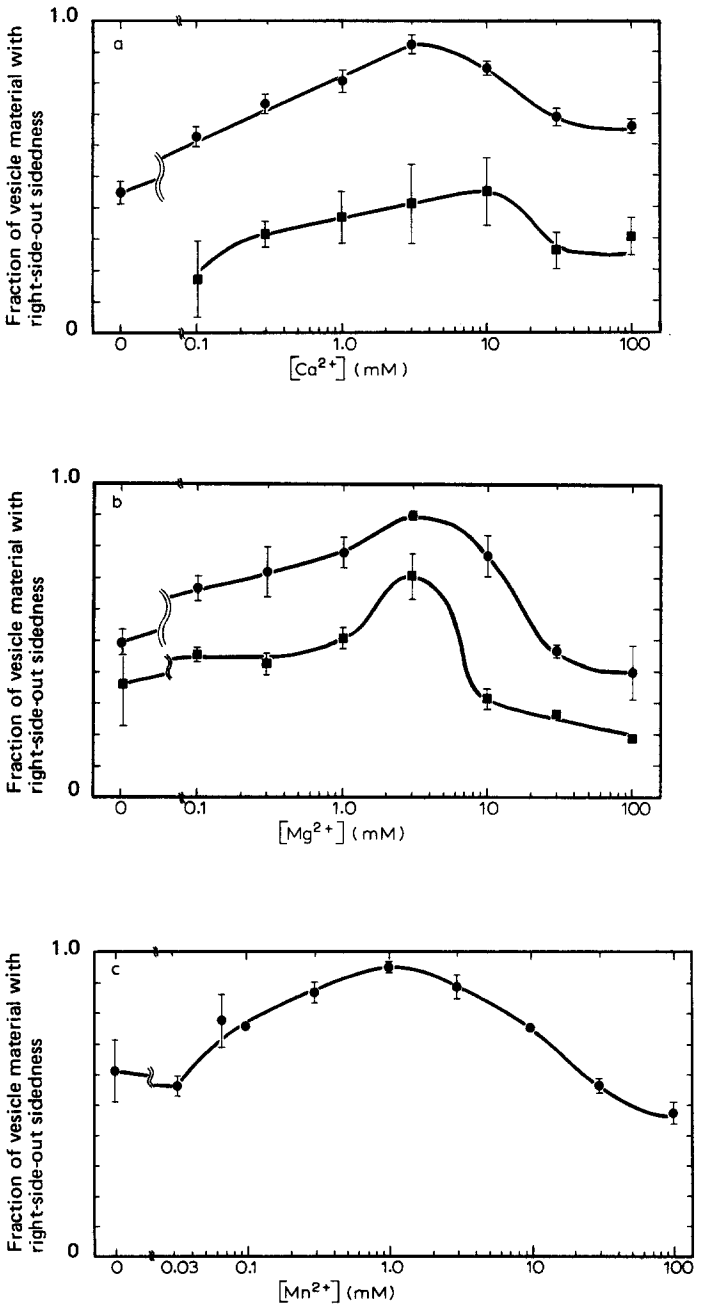

Fig. 2. Experimental fractions of vesicles which are right-side-out or unsealed (●) and sealed right-side-out only (■) as a function of bulk divalent cation concentration used in the vesiculation procedure. The former data points represent the fractions of vesicles in which the membrane B-face surface is accessible to neuraminidase action; the latter represent the fractions of vesicles in which the membrane A-face is not accessible to the assay for cytochrome *c* oxidoreductase activity. The gap between the two curves may then be taken to be the fraction of vesicles which are unsealed after vesiculation. Experiments were done in the presence of varying concentrations of (a) Ca^{2+}, (b) Mg^{2+}, and (c) Mn^{2+}. Vertical bars represent standard errors.

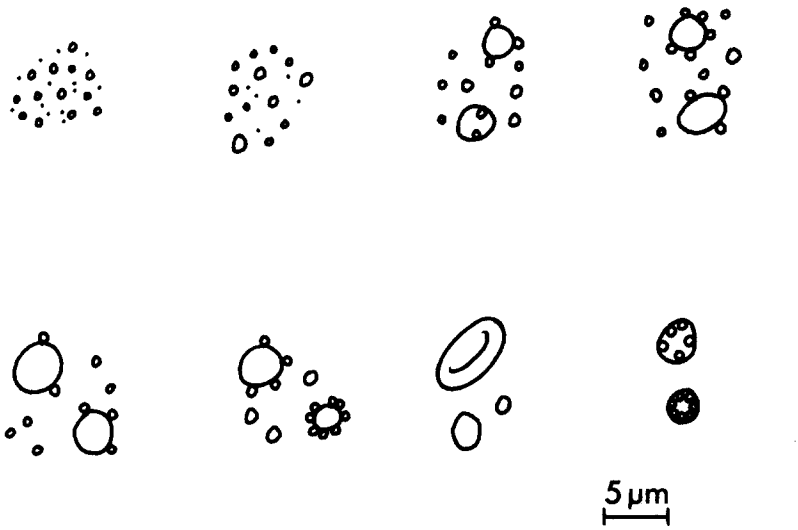

Fig. 3. Vesicle size and morphology after syringe vesiculation in Ca^{2+} or Mg^{2+} concentrations of (from left to right, top row, mM) 0, 0.1, 0.3, 1.0; (bottom row) 3.0, 10, 30, and 100. Observations were made by phase contrast microscopy.

that appear to induce small radii of curvature, a typical structure consists of a single large vesicle to which one or more small 0.1—0.5 μm blebs are attached. It may be useful to refer to these as "parent" vesicles and "daughter" vesicles (derived from blebs), respectively. Three lines of evidence support the concept of daughter vesicle formation by blebbing from parent membranes. First, the bulges on parent vesicles as seen by phase contrast microscopy have been confirmed to take on a distinct bleb morphology (i.e. spherical with a small neck) as seen by freeze-fracture electron microscopy (Fig. 4). The neck is the obvious weak link at which the bleb may break off (either by shearing or by membrane fusion), giving rise to a free daughter vesicle. Second, there is a consistent inverse relationship between the number of blebs attached to a given parent and the size of the parent itself. This apparent conservation of membrane material clearly suggests that the attached structures are derived from the parent vesicle and are not the result of vesicle agglutination. Third, the same free energy considerations that favour bilayer formation prefer maintenance of bilayer continuity (i.e. a closed surface) over exposed bilayer edges where the hydrophobic interior must come in contact with the aqueous medium. As in the case of living cells that secrete, endocytose and divide, membrane fusion is the thermodynamically preferred pathway for daughter vesicle formation. Since blebbing involves no free energy change due to transfer between hydrophobic and hydrophilic environments, it might be expected to occur spontaneously even in the absence of applied shear stress. This has, in fact, been observed by phase contrast microscopy in many experiments prior to syringe vesiculation.

Analysis of size parameters

The parent/daughter distinction suggests that there are two discrete relevant

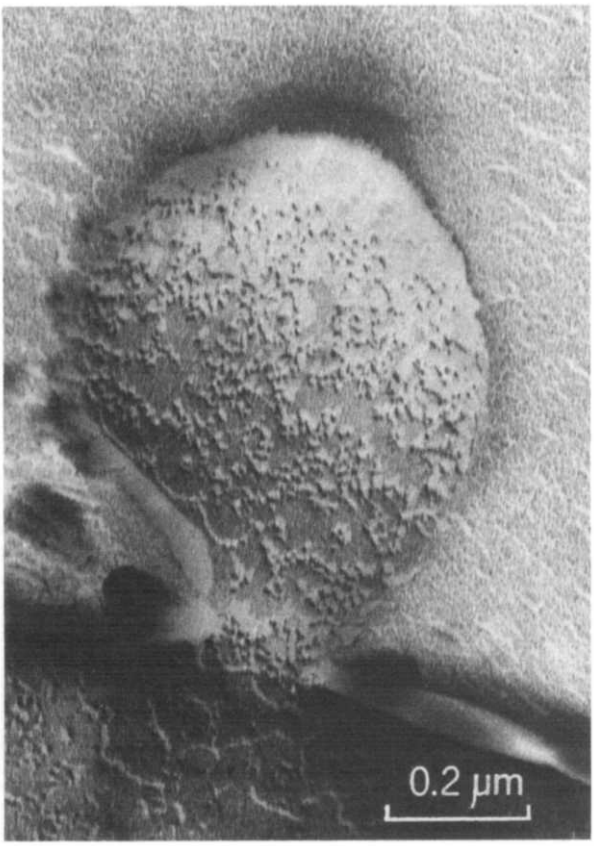

Fig. 4. External bleb from human erythrocyte membrane in 0.1 mM Mg^{2+} as seen by freeze-fracture electron microscopy. A convex A-face is shown, indicating that this is the precursor of a right-side-out daughter vesicle.

size parameters: (1) the size of the parent vesicles, and (2) the radius of curvature of daughter vesicles and blebs. It is reasonable to assume that most parent membranes are right-side-out, indeed some retain the characteristic erythrocyte dimple (biconcavity). It follows then that if the attached daughter vesicles are blebs or were created by blebbing, then the external ones are right-side-out and the internal ones inside-out. The observed correlation of external daughter vesicles with the right-side-out sidedness peaks and of internal ones with significant inside-out sidedness is clearly seen by comparing Figs. 3 and 2.

It is convenient to define the radius of curvature as positive in the right-side-out case and negative in the inside-out case (going to infinity for perfectly flat bilayers). Of the two distinct vesicle size parameters, the radius of curvature of daughter vesicles and blebs appears to be most closely associated with sidedness, external blebs having a small positive radius of curvature, internal blebs having a small negative one, and large parent vesicles with no blebs having a large radius of curvature. The simultaneous presence of right-side-out and inside-out vesicles suggests that bleb formation and vesicle inversion are probabilistic occurrences.

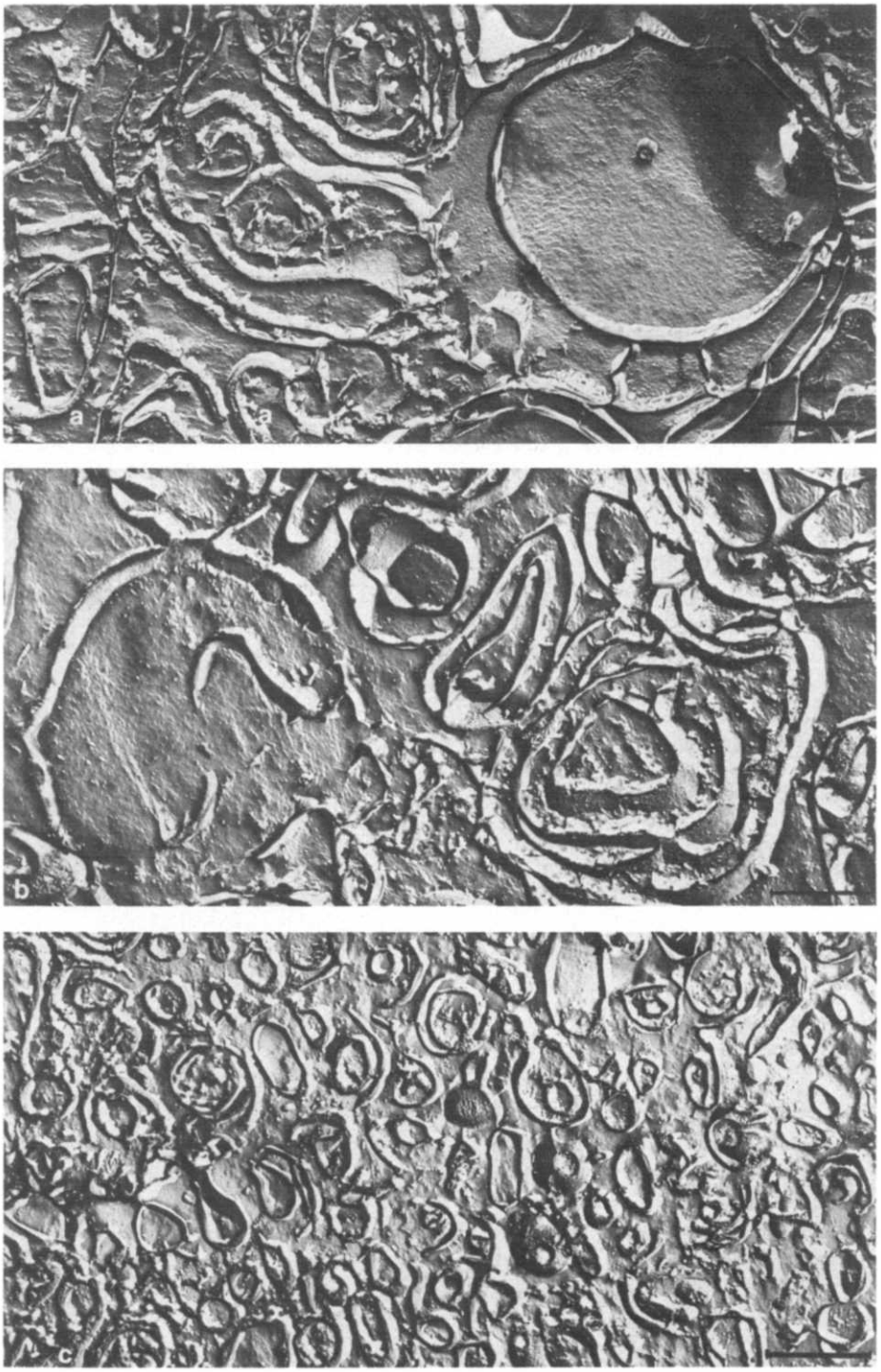

Fig. 5. Freeze-etch electron micrographs of unvesiculated erythrocyte ghosts (a), membranes which have been syringe vesiculated in 1.0 mM Ca^{2+} (b), and membranes which have been syringe vesiculated in 2.0 mM K^{+} (c). Bar = 1.0 μm.

TABLE II

VESICLE SIZE DISTRIBUTION AFTER SYRINGE VESICULATION IN THE PRESENCE OF VARIOUS CONCENTRATIONS OF Ca^{2+}

Vesicle diameter d is in μm; numbers following ± are standard errors.

$[Ca^{2+}]$ (mM)	Percent of vesicles in size range		Median size in the range $d \geqslant 2.1$
	$0.1 < d < 2$	$2 \leqslant d \leqslant 7$	
0	100 ± 0	0	—
0.1	98 ± 1.0	2 ± 1.0	2.37
0.3	90 ± 5.4	10 ± 5.4	2.63
1.0	85 ± 6.1	15 ± 6.1	2.85
3.0	55 ± 7.5	45 ± 7.5	3.06
10	44 ± 3.8	56 ± 3.8	3.90
30	25 ± 8.7	75 ± 8.7	3.09 *
100	20 ± 0.5	80 ± 0.5	2.78 *

* Decrease in diameter (calculated from vesicle volume measurements) due in part to collapse of some vesicles.

Parent vesicle size increases with divalent cation concentration until high concentrations on the order of 10 mM (Table II). Freeze-etch electron microscopy confirms phase contrast observations showing that unvesiculated ghosts (Fig. 5a) undergo little disruption after syringe vesiculation in the presence of 1.0 mM Ca^{2+} (Fig. 5b), but are considerably broken down in the absence of divalent cations in spite of the presence of 2.0 mM K^+ (Fig. 5c). Moderate divalent cation concentrations not only increase membrane resistance to fragmentation but appear to partially inhibit shearing off of blebs. The available evidence suggests that divalent cations strongly stabilise erythrocyte membranes and monovalent cations weakly stabilise, and that the degree of stabilisation is a monotonically increasing function of cation concentration in the range studied.

Discussion

Role of asymmetrically distributed membrane lipids in cation binding

Ghosts prepared by the method of Dodge et al. [22], are unsealed [21,24] and permeable to metal cations. Because they are incubated in test media for at least 1 h before vesiculation, it is reasonable to assume identical cation concentrations on either side of the bilayer. Under these conditions preferences for positive or negative radii of curvature can exist only if the bilayer is itself asymmetric.

There is now convincing evidence that this is the case with respect to intrinsic lipids, proteins, and attached polysaccharides. Cations bind to proteins [28,29], accessible secondary phosphate groups [28], and acidic phospholipids [30—32] especially phosphotidylserine. Although intrinsic proteins may influence bilayer curvature, there is presently no reason to believe that they can account for all of the shape changes observed. We observe no difference in freeze-fracture particle distributions between stable vesicles at varying cation concentrations, and the asymmetry of protein distribution appears to be con-

served under a wide variety of ionic conditions and methods of lysis [33]. Polysaccharides, while carrying electrostatic charge, are unlikely to induce curvature because they are not intrinsic to the bilayer. Lipids, as the intrinsic structural matrix of the bilayer, remain the most likely candidates.

While the data on lipid distribution in human erythrocytes [17,18,34—38] vary, the most consistent conclusion is that essentially all acidic phospholipids (phosphatidylserine, phosphatidylinositol, and phosphatidic acid) are localised in the cytoplasmic monolayer, constituting about 11 mol % of the total membrane lipid. Cations have only a slight affinity for neutral phospholipids at physiological pH, but they do bind readily to acidic phospholipids [31,32,39—43]. Thus, A-face acidic phospholipids are likely vehicles for cation-induced curvature preferences of membranes. Existing evidence suggests mechanisms by which this may take place.

Mechanisms of induction of bilayer curvature

It has been proposed that asymmetric membranes behave as bilayer couples [44], i.e. the expansion or contraction of one layer relative to the other induces a structural curvature. This hypothesis can be applied to the binding of monovalent (M^+) and divalent (M^{2+}) cations to bilayers containing acidic phospholipids (PL^-). Consider first the three conceivable binding configurations with M^{2+}: PL^- (unbound), PLM^+ (singly-bound), and PL_2M (crossbridged). An excess of either PL^- or PLM^+ results in some net electrostatic repulsion among like-charged headgroups with consequent expansion of the layer at the headgroup region. On the other hand, nearly equal quantities of PL^- and PLM^+ favour the formation of PL_2M in which the two headgroups are not only electrostatically neutralised, but also brought closer together than two unbound headgroups. As a result, the mean headgroup cross-sectional area is contracted. This is supported by experiments on phosphatidylcholine monolayers exposed to Ca^{2+} [31,32] in which a drop in surface pressure is observed. With cations binding primarily to acidic phospholipids localised in the A-face, the PL^- and PLM^+ configurations found at concentration extremes of M^{2+} induce a negative preferential radius of curvature, giving rise to stomatocytes and inside-out vesicles. Dominance of the PL_2M complex results in a positive radius of curvature as seen in echinocytes and right-inside-out vesicles (Fig. 6).

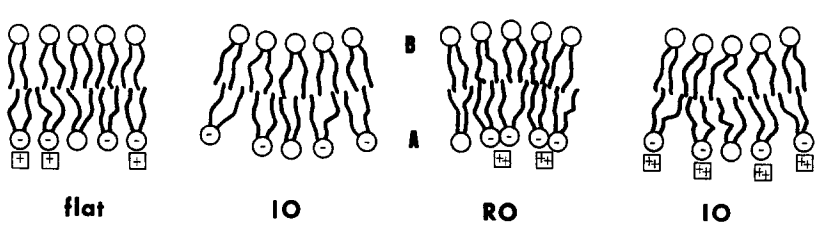

Fig. 6. Bilayer curvature as a function of ionic environment. (a) Monovalent cations (⊕) neutralise most of the otherwise negatively charged headgroups (⊖) of acidic phospholipids in the A-face (lower layer) keeping bilayer flat. (b) Absence of cations leaves a negative surface charge resulting in headgroup repulsion, A-face expansion, and inside-out (IO) curvature. (c) Some divalent cations (⊞) crossbridge adjacent headgroups resulting in A-face contraction and right-side-out (RO) curvature. (d) Divalent cation saturation of acidic headgroup binding sites creates a positive surface charge resulting in A-face expansion and inside-out curvature.

This model was also suggests why phosphatidylserine bilayer films rupture with Ca^{2+} added to only one side [45,46]. At intermediate concentrations of Ca^{2+} the PL_2M complex will dominate on one side. On the other side, PL^- is the characteristic form. The simultaneous contraction of one layer and expansion of the other induce a curvature in the planar film which disrupts bilayer continuity, resulting in breakage into small vesicles. Furthermore, addition of Ca^{2+} to both sides restores symmetry and restabilises the membrane.

In the case of M^+, there are just two possible configurations: PL^- and PLM. Lacking the contractive crossbridging configuration, there is never any great preference for echinocytic transformation or right-side-out vesicles, which is consistent with our observations (Fig. 1).

Binding stoichiometry

For M^{2+}, the cation-phospholipid binding configurations may be expressed terms of M^{2+} : PL^- binding stoichiometries: 0 : 1, 1 : 2 and 1 : 1 for PL^-, PL_2M and PLM^+, respectively. The model predicts maximisation of 1 : 2 stoichiometry at right-side-out peaks indicated in Fig. 2, and dominance of 0 : 1 and 1 : 1 stoichiometries at right-side-out valleys associated with cation concentration extremes. With maximum occurrence of 1 : 2 stoichiometry at 1—4 mM concentrations of M^{2+}, our results are consistent with most observations of 1 : 2 stoichiometry cited. They are also consistent with the greatest promotion of cell fusion at Ca^{2+} concentrations of 1 mM or more (discussed in introduction) since the 1 : 2 stoichiometry is associated with the smallest positive radius of curvature which is needed for close apposition of cell membranes to be fused. In the case of M^+, the 1 : 1 stoichiometry is not associated with any sidedness preference. Since no contraction or expansion of a layer is involved, the bilayer will have no tendency to change its curvature.

The model assumes that stoichiometries of 1 : 2 and 1 : 1 actually occur in bilayers containing acidic phospholipids. Maximum binding stoichiometries between Ca^{2+} and phosphatidylserine of 1 : 2 [32,39,40], at least 0.7 : 1 [42], and 1 : 1 [31,43] have been reported. Of those claiming a 1 : 2 maximum, one [40] was based on the separation of lipids in chloroform/methanol from proteins in the aqueous phase. Since it is unlikely that a positively charged 1 : 1 complex will enter the non-polar phase, it is not surprising that the observed Ca^{2+} : phosphatidylserine binding stoichiometry did not exceed 1 : 2, the excess Ca^{2+} being left behind in the aqueous phase. Two other reports of 1 : 2 stoichiometry [32,39] did not involve Ca^{2+} concentrations above 1 mM. Thus, the evidence suggests that 1 : 2 stoichiometry is achieved at around 1 mM, and 1 : 1 stoichiometry is approached at higher concentrations of Ca^{2+} under conditions used in our experiments. A 1 : 1 stoichiometry has also been reported for Mn^{2+} binding [43].

Finally, it should be re-emphasised that verification of the phospholipid shape hypothesis for bilayer couple curvature requires that the effect be demonstrated in protein-free bilayers. Until then, a role for intrinsic membrane proteins in these effects cannot be ruled out. Moreover, comparison of data from whole cells and ghosts must be treated with caution because, in the former, extrinsic proteins and microfilaments may be expected to contribute to cell surface morphology. Nevertheless, it is now reasonable to add membrane phos-

pholipids in association with metal cations to the list of determinants of biological membrane morphology.

Acknowledgements

This investigation was supported by U.S.P.H.S. Grant No. 5 T01 GM00829 from the National Institute of General Medical Sciences, N.I.H. Grant No. GM 18819, and N.S.F. Grant No. GB-38-359.

References

1 Lucy, J.A. (1970) Nature 227, 814—817
2 Satir, B., Schooley, C.S. and Satir, P. (1973) J. Cell Biol. 56, 153—176
3 Lau, A.L.Y. and Chan, S.I. (1975) Proc. Natl. Acad. Sci. U.S. 72, 2170—2174
4 Cohn, Z.A. (1975) Fed. Proc. 34, 1725—1729
5 Deuticke, B. (1968) Biochim. Biophys. Acta 163, 494—500
6 Sheetz, M.P., Painter, R.G. and Singer, S.J. (1976) J. Cell Biol. 70, 193—203
7 Weed, R.I. and Chailley, B. (1972) Nouv. Rev. Fr. Hématol. 12, 775—788
8 Johnson, R.M. and Robinson, J. (1976) Biochem. Biophys. Res. Commun. 70, 925—931
9 Wilkins, D.J. and Bangham, A.D. (1964) J. Reticuloendothel. Soc. 1, 233—242
10 Düzgüneş, N. and Ohki, S. (1977) Biochim. Biophys. Acta 467, 301—308
11 Poste, G. (1970) Microbios 2, 227—239
12 Ahkong, Q.F., Tampion, W. and Lucy, J.A. (1975) Nature 256, 208—209
13 Zakai, N., Kulka, R.G. and Loyter, A. (1976) Nature 263, 696—699
14 Foreman, J.C., Mongar, J.L. and Gomperts, B.D. (1973) Nature 245, 249—251
15 Cochrane, D.E. and Douglas, W.W. (1974) Proc. Natl. Acad. Sci. U.S. 71, 408—412
16 Papahadjopoulos, D., Poste, G., Schaeffer, B.E. and Vail, W.J. (1974) Biochim. Biophys. Acta 352, 10—28
17 Verkleij, A.J., Zwall, R.F.A., Roelofsen, B., Comfurius, P., Kastelijn, D. and van Deenen, L.L.M. (1973) Biochim. Biophys. Acta 323, 178—193
18 Gordesky, S.E. and Marinetti, G.V. (1973) Biochem. Biophys. Res. Commun. 50, 1027—1031
19 Renooij, W., van Golde, L.M.G., Zwaal, R.F.A. and van Deenen, L.L.M. (1976) Eur. J. Biochem. 61, 53—58
20 Gent, W.L.G., Trounce, J.R. and Walser, M. (1964) Arch. Biochem. Biophys. 105, 582—589
21 Steck, T.L. and Kant, J.A. (1974) Methods Enzymol. 31A, 172—180
22 Dodge, J.T., Mitchell, C. and Hanahan, D.J. (1963) Arch. Biochem. Biophys. 100, 119—130
23 Warren, L. (1959) J. Biol. Chem. 234, 1971—1975
24 Steck, T.L. (1974) in Methods in Membrane Biology (Korn, E.D., ed.), Vol. 2, pp. 245—281, Plenum Press, New York
25 Zamudio, I., Cellino, M. and Canessa-Fischer, M. (1969) Arch. Biochem. Biophys. 129, 336—345
26 Warburg, O. and Christian, W. (1942) Biochem. Z. 310, 384—421
27 Lowry, O.H., Rosebrough, N.J., Farr, A.L. and Randall, R.J. (1951) J. Biol. Chem. 193, 265—275
28 Sanui, H. and Pace, N. (1962) J. Cell. Comp. Physiol. 59, 251—257
29 Tolberg, A.B. and Macey, R.I. (1972) J. Cell. Physiol. 79, 43—51
30 Abramson, M.B., Katzman, R. and Gregor, H.P. (1964) J. Biol. Chem. 239, 70—76
31 Rojas, E. and Tobias, J.M. (1965) Biochim. Biophys. Acta 94, 394—404
32 Papahadjopoulos, D. (1968) Biochim. Biophys. Acta 163, 240—254
33 Bretscher, M.S. (1973) Science 181, 622—629
34 Rothman, J.E. and Dawidowicz, E.A. (1975) Biochemistry 14, 2809—2816
35 Poznansky, M. and Lange, Y. (1976) Nature 259, 420—421
36 Fisher, K.A. (1976) Proc. Natl. Acad. Sci. U.S. 73, 173—177
37 Rouser, G., Nelson, G.J., Fleischer, S. and Simon, G. (1968) in Biological Membranes: Physical Fact and Function (Chapman, D., ed.), pp. 5—69, Academic Press, London
38 Turner, J.D. and Rouser, G. (1970) Anal. Biochem. 38, 423—436
39 Bangham, A.D. and Papahadjopoulos, D. (1966) Biochim. Biophys. Acta 126, 181—184
40 Forstner, J. and Manery, J.F. (1971) Biochem. J. 124, 563—571
41 Duffy, M.J. and Schwarz, V. (1973) Biochim. Biophys. Acta 330, 294—301
42 Joos, R.W. and Carr, C.W. (1967) Proc. Soc. Exp. Biol. Med. 124, 1268—1272
43 Hauser, H., Darke, A. and Phillips, M.C. (1976) Eur. J. Biochem. 62, 335—344
44 Sheetz, M.P. and Singer, S.J. (1974) Proc. Natl. Acad. Sci. U.S. 71, 4457—4461
45 Papahadjopoulos, D. and Ohki, S. (1969) Science 164, 1075—1077
46 Ohki, S. (1972) Biochim. Biophys. Acta 255, 57—65